ACS APPLIED MATERIALS & INTERFACES

Research Article

Cite This: ACS Appl. Mater. Interfaces 2019, 11, 11349−11359

www.acsami.org

Construction of Novel Enzyme−Graphene Oxide Catalytic Interface with Improved Enzymatic Performance and Its Assembly Mechanism

Yongzhi Chen,[†] Zhigang Luo,*[,†,‡,§] and Xuanxuan Lu[∥]

[†]School of Food Science and Engineering, South China University of Technology, Guangzhou 510640, China

[‡]South China Institute of Collaborative Innovation, Dongguan 523808, China

[§]Overseas Expertise Introduction Center for Discipline Innovation of Food Nutrition and Human Health (111 Center), Guangzhou 510640, China

[∥]Department of Food Science, Rutgers, The State University of New Jersey, 65 Dudley Road, New Brunswick, New Jersey 08901, United States

Supporting Information

ABSTRACT: In the present study, a novel bioinorganic catalytic interface, combining the in situ radical polymerization technique with the noncovalent adsorption method, was successfully fabricated, and its assembly mechanism was explored. The in situ radical polymerization technique was applied to construct a polymer shell around the enzyme surface to form the protein nanocapsule. Then, protein nanocapsules assembled on the surface of graphene oxide (GO) through noncovalent interactions to fabricate the dual-immobilized enzyme system. Here, native organophosphorus hydrolase (OPH) and OPH nanocapsule (nOPH10) were immobilized on GO to form the traditional immobilized OPH (OPH@GO) and dual-immobilized OPH (nOPH10@GO), respectively. The introduced polymer shell could protect the enzyme from various denaturation factors and provide abundant functional groups to interact with supports to strengthen the interactions between them. Compared to native OPH and OPH@GO, the resulting nOPH10@GO exhibited enhanced catalytic activity, stability, and reusability. The nOPH10@GO was further used to construct the biosensor, which exhibited better detection performance compared with that of OPH@GO. These features indicated that the introduced enzyme immobilization system could enhance the enzymatic performance and broaden its application prospect.

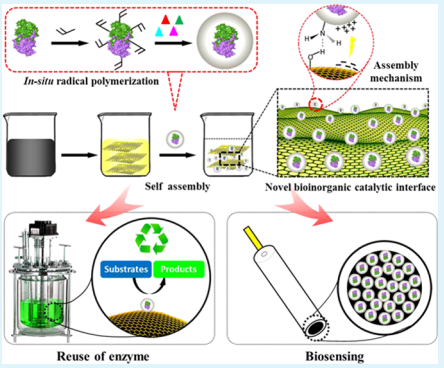

KEYWORDS: *bioinorganic catalytic interfaces, enzyme immobilization, radical polymerization, protein nanocapsule, graphene oxide, biosensing*

1. INTRODUCTION

Industrial biotechnology is consistently searching for improved enzyme performance and stability under harsh conditions in most industrial processes. As nontoxic and environmentally friendly catalysts, enzymes are widely used in environmental protection, food processing, biopharmacy, development of clean energy, and many other fields.[1−3] However, the fragile nature of enzymes restricts their application. Enzymatic catalysis is usually conducted in aqueous media and at ambient temperature. Besides, the requirements of low costs, high loadings, and reusability in commercial production also limit the application of free enzymes.[4] Enzyme immobilization is an effective approach to improve the stability and reusability of enzymes in solution, making them commercially and industrially viable. To construct a robust immobilized enzyme, searching for a suitable supporting matrix is one of the important steps.[5,6] The supporting materials should meet the demands for biocompatibility, stability, and high enzyme loadings.[7,8] Recently, graphene oxide (GO) has attracted wide attention due to its incredibly large specific surface area (single-layered and unique double-sided material), abundant oxygen-containing functional groups (such as hydroxyl, carbonyl, carboxyl, and epoxy groups), and high biocompatibility.[9,10] These unique physical and chemical properties make GO an outstanding supporting matrix for enzyme immobilization. Zhang et al. reported that the enzyme could be readily immobilized on GO without using any cross-linking reagents or additional surface modification.[11] GO and their derivates also show broad application prospects in the fields of biomedicine and electronic devices.[12−14]

Choosing a suitable immobilization method is another important aspect when constructing a robust immobilized enzyme.[8] Until now, to meet the burgeoning demands of green and sustainable chemistry, an increasing number of enzyme immobilization methods have been developed with application in various chemical transformation and industrial production,

Received: November 26, 2018
Accepted: March 7, 2019
Published: March 7, 2019

DOI: 10.1021/acsami.8b20744
ACS Appl. Mater. Interfaces 2019, 11, 11349−11359

Scheme 1. Construction of Novel Bioinorganic Catalytic Interfaces

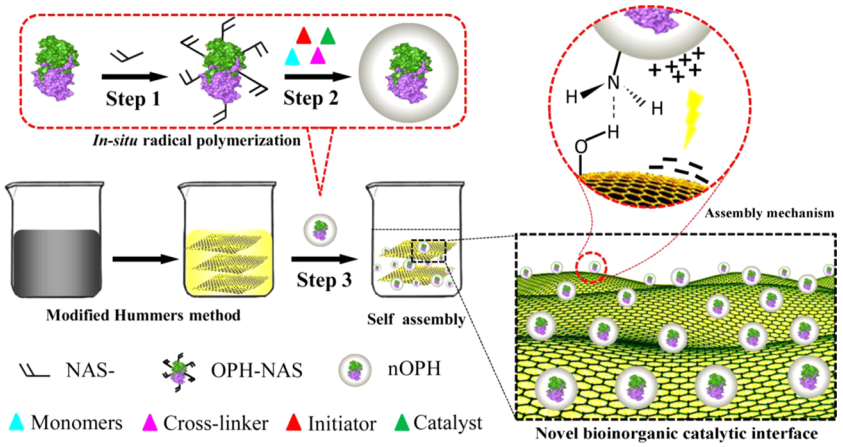

and their rise in popularity among the catalysis community has been unprecedented.[15−17] Basically, the methods for enzyme immobilization could be categorized into three types: encapsulation, cross-linking method, and support binding.[18−20] Each has its own advantages and disadvantages. Encapsulation is usually achieved via inclusion of an enzyme into a polymer network (organic polymer or silica sol−gel) or a membrane device (hollow fiber or microcapsule).[21] This method can maintain the most enzyme activity. But it is difficult to obtain a good match between the supporting material and the enzyme size. Enzymes with sizes equal to or larger than that of the host system result in low loadings, whereas those with sizes much smaller than that of the host material can easily leach out from the host.[20,22] The cross-linking method involves the addition of cross-linking reagents and intense chemical reaction during the preparation process, thereby leading to great loss of enzyme activity.[8,23] Support binding can be fulfilled via a covalent bond or noncovalent (hydrophobic interaction and van der Waals interaction) interaction.[20] Noncovalent adsorption of enzymes onto a supporting material is the simplest method for enzyme immobilization, which has already been used in industrial applications.[24,25] This method could maintain most of the enzyme activity. However, its environmental stability is unsatisfying.[1,20] The reason is that enzymes are adsorbed on the surface of the supporting material and exposed to surrounding environments directly, and therefore the environmental temperatures, organic solvents, heavy metal ions, and acidic or basic levels can severely influence the enzyme activity and stability.[26] Overall, developing an immobilized method that can retain high enzyme activity with high environmental stability is highly essential but challenging.

Here, a novel bioinorganic catalytic interface was first fabricated to surmount the disadvantages of traditional immobilized enzymes. As illustrated in Scheme 1, the in situ radical polymerization technique was applied to construct the polymer shell around the enzyme surface. First, enzymes were conjugated with polymerizable acryl groups by grafting their lysine residues with *N*-acryloxysuccinimide (NAS) (step 1).[27,28] Subsequently, a thin permeable layer of polymer network grew around the acryloylated enzymes through radical polymerization at room temperature to form protein nanocapsules (step 2). Finally, protein nanocapsules assembled on the surface of GO through noncovalent interactions to fabricate the enzyme−graphene oxide catalytic interface (step 3). Hereinto, through the dual-immobilized process, the polymer shell could help stabilize enzyme conformation, and the GO made the recovery and reuse of protein nanocapsules viable. The proposed enzyme immobilization system can enhance the enzymatic activity and improve the operational stability.

Therefore, the objective of this work was to introduce the novel and robust dual-immobilized enzyme system and investigate its catalytic performance as well as assembly mechanism. Organophosphorus hydrolase (OPH), which could hydrolyze organophosphate pesticides (OPs), was chosen as a model enzyme since it was widely used to protect the environment from the pollution of organophosphate pesticide residues but was hampered by its fragile nature.[27,29] First, the proposed enzyme−graphene oxide catalytic interface was successfully assembled. The surface morphologies, ζ-potentials, and secondary structures of the native enzyme and the immobilized enzyme were characterized by transmission electron microscopy (TEM), atomic force microscopy (AFM), dynamic light scattering (DLS), and circular dichroism (CD) spectroscopy. UV−vis spectroscopy, Fourier transform infrared spectroscopy (FT-IR), and contact angle determination were used to reveal the immobilization mechanisms of the native enzyme and the enzyme nanocapsule on GO. Subsequently, we studied the enzymatic properties and kinetic parameters. The effect of temperature, pH, and organic solvents on the catalytic activities of native enzyme and immobilized enzyme was also explored. Finally, the storage stability, environmental stability, and reusability of the dual-immobilized enzyme and the traditional immobilized enzyme were compared. To the best of our knowledge, it is the first time that this dual-immobilized enzyme system, combining in situ radical polymerization technique with noncovalent adsorption method, has been reported. This study could provide the requisite data for the rational design of an appropriate enzyme immobilization platform, which enables enzymes with improved catalytic performance and stability in harsh industrial processes.

2. MATERIALS AND METHODS

2.1. Reagents and Materials. All chemicals were purchased from Shanghai Aladdin Bio-Chem Technology Co., LTD (Shanghai, China) unless otherwise noted. OPH was obtained from Beijing Sengen Biya Biology Engineering Technology Co., Ltd. Before using, the OPH was purified using the ammonium sulfate deposition method reported elsewhere.[30] The purity of OPH was determined by sodium dodecyl sulfate polyacrylamide gel electrophoresis (SDS-PAGE) with Coomassie Blue staining.

DOI: 10.1021/acsami.8b20744
ACS Appl. Mater. Interfaces 2019, 11, 11349−11359

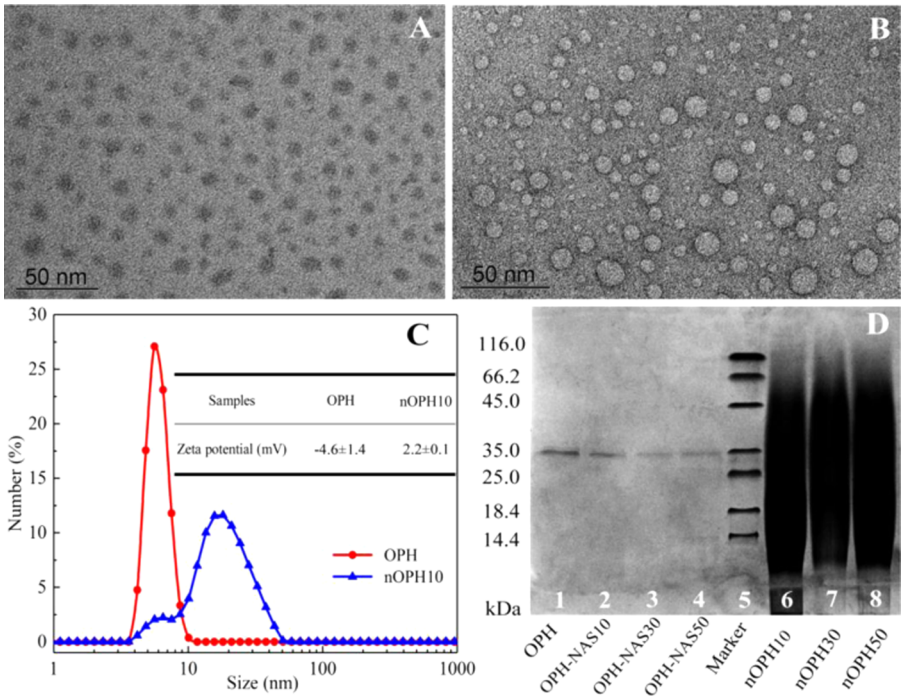

Figure 1. Representative TEM images of OPH (A) and nOPH10 (B). Particle size distributions and ζ-potentials of OPH and nOPH10 (C). Electrophoretograms of native OPH, acryloylated OPHs, and OPH nanocapsules prepared with three different NAS/OPH ratios (10:1, 30:1, and 50:1) (D).

2.2. Instruments and Methods. Transmission electron microscopy (TEM) observations were performed using JEM-1400 Plus (JEOL Ltd, Japan) at an acceleration voltage of 200 kV. Protein samples were stained using 1% pH 7.0 phosphotungstic acid (PTA) solutions before the observation. Atomic force microscopy (AFM) images were captured using a Nanoscope IIIa Multimode scanning probe microscope (Nanoscope 3A Multimode, Veeco). Particle size and ζ-potential were measured on a Nano ZS instrument (Malvern Instrument Ltd, U.K.). UV−vis adsorption was acquired on a Hanon i5 UV−vis spectrometer (Hanon Instruments Co., Ltd., China). The FT-IR spectra of support materials were acquired with KBr disks on an FT-IR spectrometer (Bruker Co., Germany). The contact angles were obtained on a DCa40 MICRO system (DATA Physics, Germany). The circular dichroism (CD) spectra were acquired by CD spectroscopy (Applied Photophysics Chirascan, U.K.) at room temperature. Lyophilized samples were obtained by using a Scientz-10 N freeze-dryer (Ningbo Scientz Biotechnology Co., Ltd, China).

2.3. Preparation of OPH Nanocapsules. First, 40 mg of OPH was dissolved into 10 mL of 50 mM pH 8.0 phosphate buffered saline (PBS). OPHs were then conjugated with polymerizable acryl groups by grafting their lysine groups with *N*-acryloxysuccinimide (NAS) at a reaction temperature of 4 °C for 2 h. The NAS/OPH molar ratio was 10:1, and the resulting acryloylated OPH was denoted OPH-NAS10. Then, in situ radical polymerization was carried out by adding monomers acrylamide (AAM) and *N*-(3-aminopropyl) methacrylamide (APM), cross-linker *N*,*N*′-methylene bisacrylamide (BIS), initiator ammonium persulfate (APS), and catalyst *N*,*N*,*N*′,*N*′-tetramethylethylenediamine (TEMED) into the reaction solution. The mass ratio of OPH-NAS10/AAM/APM/BIS/APS/TEMED was 1:3:1.5:0.2:0.5:2. The reaction was conducted under a nitrogen atmosphere at room temperature for 2 h. Finally, the resulting OPH nanocapsule (nOPH10) was dialyzed in 50 mM pH 8.0 PBS to remove the unreacted chemicals. The concentration of purified nOPH10 was determined by a nicinchoninic acid colorimetric protein assay.[27] The concentration of nOPH10 was finally diluted to 2 mg mL^{-1} for future use. Furthermore, to synthesize the OPH nanocapsules with increasing covalent linkages between the OPH core and the polymer shell, the OPH was conjugated with increasing amounts of NAS (NAS/OPH molar ratio: 30:1 and 50:1). The resulting OPH nanocapsules were denoted nOPH30 and nOPH50, respectively. Other OPH nanocapsules with different ζ-potentials were synthesized by adjusting the mass ratios of protein to different monomers. Specifically, OPH was first conjugated with NAS at the NAS/OPH molar ratio of 10:1. Then, OPH nanocapsules were synthesized using different AAM/APM mass ratios (1:3, 2:2, 3:1, and 4:0; OPH was rated as 1) as comonomers. The reaction conditions and other processes were the same as the above experiment. These OPH nanocapsules were denoted $nOPH10_{(1:3)}$, $nOPH10_{(2:2)}$, $nOPH10_{(3:1)}$, and $nOPH10_{(4:0)}$, respectively.

2.4. Preparation of Supporting Materials and Immobilized Enzymes. GO sheets were prepared according to the modified Hummers method.[31,32] To obtain the GO sheets with different reduction degrees, the GO was then reduced by L-ascorbic acid (L-AA) for 2 and 24 h, respectively, denoted rGO2h and rGO24h. The processes of immobilizing OPH and nOPH10 on GO were carried out by simply mixing the enzymes with GO solutions. Briefly, 2 mL of GO dispersion (2 mg mL^{-1}) was mixed with varying volumes of enzyme solution (2 mg mL^{-1}). The volume ratios of enzymes/GO were 0.5:1, 1:1, 1.5:1, 2:1, 2.5:1, and 3:1. All mixtures were adjusted to a final volume of 8 mL by adding an appropriate volume of PBS (50 mM, pH 8.0). The mixed solution was kept at 4 °C for 12 h. Subsequently, the mixture was centrifuged at 10 000 rpm for 10 min, and the supernatant was carefully collected to determine the enzyme loading and loading efficiency. The solids were washed thoroughly to remove the free OPH. The resulting immobilized enzymes were stored at 4 °C for future use. The preparations of nOPH30@GO and nOPH50@GO were similar to the above processes.

2.5. Determination of Enzymatic Properties and Kinetic Parameters. The enzymatic activity was determined by monitoring the absorbance change at 405 nm in 50 mM pH 8.0 PBS at 37 °C by using parathion-methyl as the substrate. The specific activity of native OPH was set to 100%. The study of Michaelis−Menten kinetics was carried out with various substrate concentrations. The Michaelis constant (K_m) and maximum reaction rate (V_{max}) were obtained from the double-reciprocal plot. The catalytic constant (k_{cat}) was calculated from the ratio of V_{max} to enzyme concentration.

DOI: 10.1021/acsami.8b20744
ACS Appl. Mater. Interfaces 2019, 11, 11349−11359

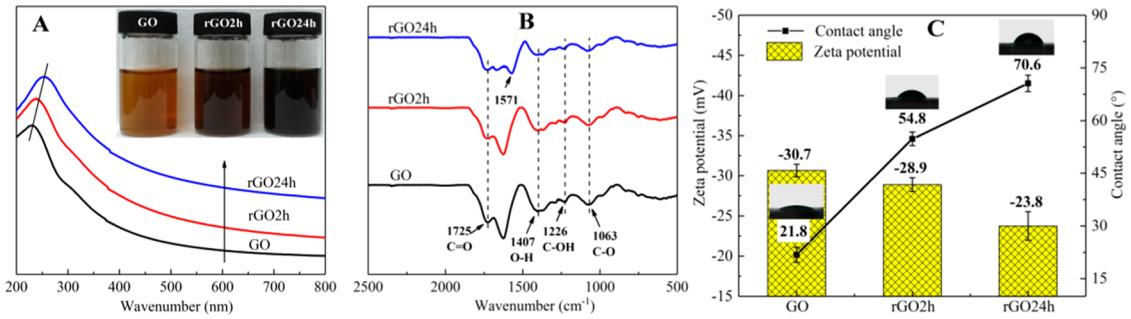

Figure 2. UV−vis spectra (A); photographs (inset of A) and FT-IR spectra (B) of the GO, rGO2h, and rGO24h; and the water contact angles and ζ-potentials of rGOs (C).

2.6. Environmental and Storage Stabilities. Thermal stabilities of native OPH, OPH@GO, and nOPH10@GO were carried out in a 65 °C water bath. The organic solvent tolerance tests were performed through exposure of enzymes in 50 mM pH 8.0 PBS containing different fractions of methanol or dimethyl sulfoxide (DMSO) (volume fraction from 5 to 20%). The adaptabilities of native OPH, OPH@GO, and nOPH10@GO in PBS (50 mM) with different pH values (6−10) were assayed. The freeze−thaw stabilities of native OPH and immobilized OPH were measured by subjecting them to freeze−thaw cycles. The native OPH and immobilized OPH were stored at 4 °C for different times, and then, the residual activity of the enzyme was assayed as the above-described method.

2.7. Reusability of Traditional and Dual-Immobilized Enzyme. To study the reusabilities of OPH@GO and nOPH10@GO, these two immobilized enzymes were readily recycled by centrifugation at the end of each cycle and washed three times with PBS (50 mM, pH 8.0) before the next cycle. The specific activity of each immobilized enzyme at the first run was set to 100%.

2.8. Application in Biosensor. The traditional immobilized enzyme and the dual-immobilized enzyme were applied to construct biosensors. The preparation of OPH@GO and nOPH10@GO modified glassy carbon electrode (GCE) surface was based on the reported procedure with some slight modifications.[33,34] Specifically, the bare GCE (diameter: 3 mm) was successively polished with 0.3 and 0.05 μm alumina slurry and then sonicated with ethanol and distilled water for 3 min to remove any alumina residue on the electrode surface. Subsequently, nOPH10@GO was uniformly dispersed in appropriate volume of PBS (50 mM, pH 8.0) to obtain a final concentration of 20 mg mL^{-1}. Here, 6.0 μL of the suspension was carefully dropped onto the bare GCE surface and dried at room temperature (25 °C). Finally, 6.0 μL of Nafion solution (0.05 wt %) was syringed onto the surface of the modified electrode and dried at room temperature to strengthen the stability. The electrode was denoted nOPH10@GO/GCE. The preparation of OPH@GO and GO modified GCE surface was similar to the above processes. These two electrodes were denoted OPH@GO/GCE and GO/GCE, respectively. The electrochemical behavior of the prepared electrodes was characterized by cyclic voltammetry (CV). The experiments were performed on the CHI 660D electrochemical workstation (Shanghai Chenhua Co., China) at room temperature with a three-electrode system using the bare GCE or modified GCE as the working electrode, the platinum wire as the counter electrode, and the saturated calomel electrode as the reference electrode. The prepared electrodes were kept in a refrigerator (at 4 °C) when not in use.

3. RESULTS AND DISCUSSION

3.1. Characterization of OPH and OPH Nanocapsules. The successfully constructing polymer shell on the enzyme surface is the key to the construction of bioinorganic catalytic interfaces. The polymer shell can protect the enzyme from various denaturation factors. Moreover, it provides numerous functional groups, which can interact with the support surface to improve the stability of the immobilized enzyme. Various characterization techniques were used to confirm the formation of nOPH10. Figure 1A,B show the representative transmission electron microscopy (TEM) images of native OPH and nOPH10. It could be seen that the surface morphology of OPH was significantly changed after the formation of the polymer shell around its surface. Native OPH with uniform size exhibited a dark shadow without a distinct outline. This may due to the fact that OPH was stained using PTA before the observation, in which the PTA could combine with tyrosine and tryptophan residues in the proteins.[35−37] The heavier atoms in PTA are more capable of blocking the scattering electron compared with these lighter atoms in protein,[35,37] so the PTA stained proteins presented the above appearance under the TEM observation. By comparison, nOPH10 presented a spherical morphology and a wider size distribution. This difference suggested that the polymer shell was successfully assembled around the enzyme surface. As evidence, Figure 1C shows particle size distributions and ζ-potentials of native OPH and nOPH10 measured by dynamic light scattering (DLS). The native OPH showed negative charge (−4.6 mV) with a size distribution centered at 5.6 nm, which was consistent with the previous reported molecular dimension (6.1 nm × 8.6 nm × 5.1 nm).[27,38] However, the nOPH10 presented a positive charge about 2.2 mV and a wider size distribution from 5 to 50 nm, indicating that the polymer shell increased the enzyme size.

The successful assembly of the polymer shell was also confirmed by SDS-PAGE. Figure 1D shows the electrophoretograms of nOPH10 (stripe 6), nOPH30 (stripe 7), and nOPH50 (stripe 8). Compared to the well-defined band of native OPH (stripe 1), OPH nanocapsules (nOPHs) were broadly dispersed within the gel (Figure 1D, stripes 6−8) possibly because polymer shells on their surface prevented them from being reduced by β-mercaptoethanol. That is to say, the disulfide bond in the nOPH structure may not be destroyed and nOPHs cannot combine very well with SDS. Thus, nOPHs remained intact during the electrophoresis and were separated according to their size, shape, and surface charge, which resulted in the broad dispersion in the gel. Similar phenomenon regarding the dispersing electrophoretogram of protein nanocapsule was also reported by Wen et al.[39] By contrast, the acryloylated OPHs (denoted OPH-NAS10, OPH-NAS30, and OPH-NAS50), which did not form the polymer shell on the enzyme surface, exhibited similar stripes (Figure 1D, stripes 2−4) to native OPH. This phenomenon further confirmed that the polymer shell was successfully assembled on the enzyme surface, and the surface property of nOPHs was obviously different from that of the OPH. Therefore, combining the results from TEM, DLS, and SDS-

DOI: 10.1021/acsami.8b20744
ACS Appl. Mater. Interfaces 2019, 11, 11349−11359

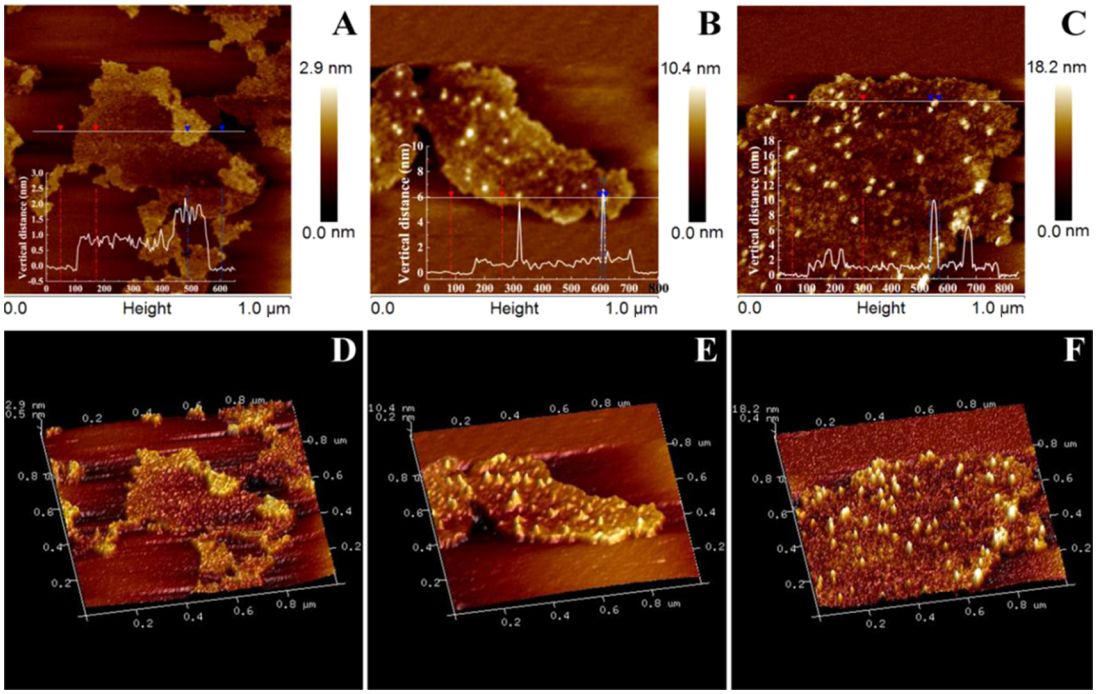

Figure 3. Representative AFM images of GO (A), OPH@GO (B), and nOPH10@GO (C) and their corresponding height profiles (insets in A–C) and 3D images (D–F).

PAGE, it is reasonable to conclude that the proposed polymer shells are successfully constructed around the enzyme surface to form the nanocapsules. Herein, cationic nOPH10 was chosen as a model to construct this system in the present study.

More importantly, precise control over the charge of protein nanocapsules can be achieved by selecting the appropriate monomer composition. OPH nanocapsules with different ζ-potentials were synthesized using different AAM/APM mass ratios (1:3, 2:2, 3:1, and 4:0) as comonomers. The ζ-potentials (Supporting Information, Figure S1) of $nOPH10_{(1:3)}$, $nOPH10_{(2:2)}$, and $nOPH10_{(3:1)}$ were 3.2, 2.3, and 2.0 mV, respectively. However, the $nOPH10_{(4:0)}$, which was synthesized using AAM as the only monomer, showed negative charge (−3.7 mV). The controllable preparation of protein nanocapsules with different properties would play an important role in the construction of a dual-immobilized enzyme system. Such a function can meet the requirement of various supports with different charges as well as different electric properties.

3.2. Characterization of GO Supports and Immobilized Enzymes. As presented in the inset of Figure 2A, the color of reduced graphene oxides (rGOs) changed from bright yellow to black with the increase in reduction degree.[10] The UV–vis absorption peak at 230 nm in GO also red-shifted to 239 and 252 nm in rGO2h and rGO24h, respectively. These results suggested that the longer the reaction time lasted, the greater the reduction degree was.[9,10] Furthermore, the absorption intensity of the entire spectrum of the rGOs gradually increased, which indicated that the GO was reduced by L-AA. The reduction of GO was further verified by FT-IR spectroscopy. As shown in Figure 2B, the spectra of graphite oxides indicated the presence of several strong characteristic peaks corresponding to the oxygen-containing functional groups, such as the C═O stretching vibration peak at 1725 cm^{-1}, O–H deformations in the C–OH groups at 1407 cm^{-1}, C–OH stretching vibration peak at 1226 cm^{-1}, and C–O stretching vibrations peak in C–O–C of the epoxide at 1063 cm^{-1}.[9,10,40] After reduction, the peak intensity of the oxygen functional groups gradually decreased, and the skeletal vibration absorption peak of graphene at about 1571 cm^{-1} was observed, indicating the successful restoration of the partial aromatic ring structure.[10]

Additionally, the hydrophobicity of the rGOs surface was enhanced compared to that of GO. As presented in Figure 2C, the water contact angles of GO, rGO2h, and rGO24h were 21.8, 54.8, and 70.6°, respectively. Apparently, these results demonstrated that the hydrophobicity of the rGOs surface was positively correlated to its reduction degree. The improved hydrophobicity of rGOs can be attributed to the removal of oxygen-containing functional groups from the GO surface through chemical reduction. Figure 2C shows that the ζ-potentials of rGO2h and rGO24h decreased to −28.9 and −23.8 mV, respectively. The ζ-potential results further confirmed the reduction of GO, which were consistent with the UV–vis absorption, FT-IR spectra, and contact angle results.

The morphologies of GO, OPH@GO, and nOPH10@GO were characterized using AFM. Figure 3A shows that the GO had a two-dimensional structure. The superimposed cross-section measurements taken along the white line indicated a sheet thickness of around 1 nm, suggesting a single atomic layer thickness structure was obtained.[32] This structure was also confirmed by TEM (Supporting Information, Figure S2), in which the GO sheet appeared transparent and was folded over on one edge with some small fragments of GO on its surface. In Figure 3B,C, the bright dots on the GO surface were OPH and nOPH10, respectively. The maximum height of nOPH10@GO (inset of Figure 3C) was higher than that of OPH@GO (inset of Figure 3B), which resulted from the polymer shell around nOPH10. A similar morphology was found in native OPH and nOPH10 (Supporting Information, Figure S3). The maximum height of nOPH10 was 17.8 nm,

DOI: 10.1021/acsami.8b20744
ACS Appl. Mater. Interfaces 2019, 11, 11349–11359

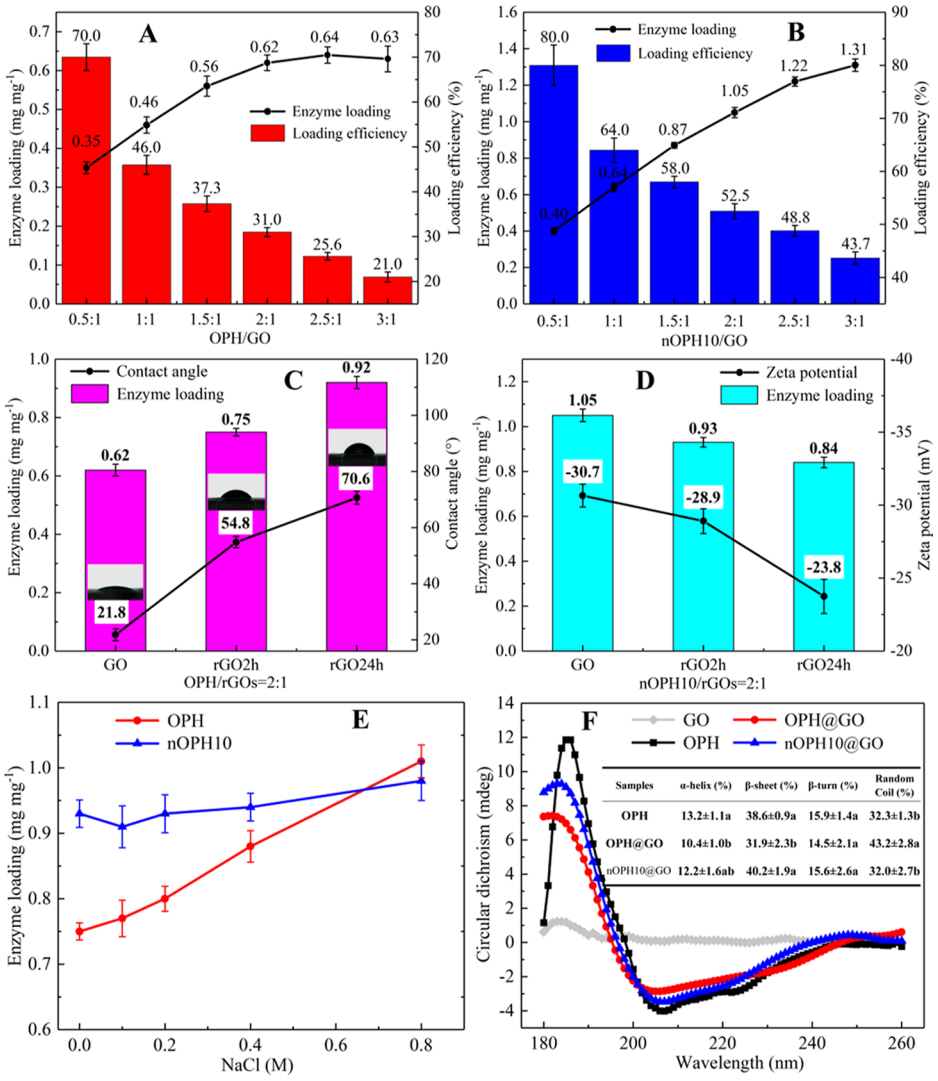

Figure 4. Enzyme loadings of native OPH (A) and nOPH10 (B) and loading efficiencies at different enzyme/GO mass ratios (0.5:1; 1:1; 1.5:1; 2:1; 2.5:1; 3:1). The water contact angles of rGOs and the loadings of OPH at OPH/rGOs mass ratio of 2:1 (C). ζ-Potentials of rGOs and the loadings of nOPH10 at nOPH10/rGOs mass ratio of 2:1 (D). Effect of the concentrations of NaCl on the loadings of native OPH and nOPH10 on rGO2h (E). CD spectra of the native and immobilized OPH and their secondary structures (F) and the loadings of OPH and nOPH10 were both 0.64 mg mg^{-1}.

greater than that of native OPH (8.7 nm). As presented in Figure S3, native OPH tended to be agglomerated (Figure S3A,C), and the nOPH10 was well dispersed (Figure S3B,D). This phenomenon may be ascribed to the protection effect of the polymer shell, which prevented the nOPH10 from being agglomerated. In addition, the three-dimensional (3D) images (Figure 3D−F) clearly indicated that many bumps appeared on the GO surface, and the surface topographies of OPH@GO and nOPH10@GO were different. The results confirmed that the bioinorganic catalytic interfaces were successfully constructed. It was noteworthy that the ζ-potential of GO (−30.7 mV) was changed dramatically after loading with enzymes (Supporting Information, Table S1). OPH@GO had a negative charge of −22.8 mV, whereas nOPH10@GO had a positive charge of 1.8 mV, indicating that the enzyme could significantly influence the GO surface properties.

3.3. Enzyme Immobilization and Its Mechanism. Figure 4A,B show the enzyme loadings and loading efficiencies of OPH and nOPH10 on GO. With the increase in the enzyme/support mass ratio (from 0.5:1 to 3:1), more OPH and nOPH10 were adsorbed on GO. Moreover, the loading efficiency of nOPH10 was higher than that of OPH. When the enzyme/support mass ratio increased to 3:1, the loading of nOPH10 increased to 1.31 mg mg^{-1}, which was more than twice higher than that of OPH (0.63 mg mg^{-1}). This could be attributed to the different surface properties between OPH and nOPH10. The ζ-potential of OPH showed a negative charge (−4.6 mV), the nOPH10 presented a positive charge (2.2 mV), and the GO exhibited a strong negative charge (−30.7 mV). Therefore, the nOPH10 was immobilized on GO mainly because of the electrostatic attraction. However, for OPH, there may be some other interactions governing the adsorption process.

To further understand the interaction between enzymes and supports, GOs with different reduction degrees were applied to immobilize OPH and nOPH10. The immobilizations of OPH and nOPH10 on rGOs were both at the enzyme/support mass ratio of 2:1. As presented in Figure 4C, the loading of OPH increased as the hydrophobicity of the rGO surface increased. This result indicated that there was a positive correlation

DOI: 10.1021/acsami.8b20744
ACS Appl. Mater. Interfaces 2019, 11, 11349−11359

Table 1. Enzymatic Properties and Kinetic Parameters of Native OPH, OPH@GO, nOPH10, and nOPH10@GO[a]

samples[bT]	relative activity (%)	K_m (μM)	k_{cat} (s^{-1})	k_{cat}/K_m (s^{-1} μM^{-1})
OPH	100.0 ± 2.5*b*	56.2 ± 4.1*b*	47.5 ± 2.9*b*	0.845
OPH@GO	90.2 ± 2.1*c*	98.4 ± 10.5*a*	52.3 ± 4.7*b*	0.532
nOPH10	97.3 ± 2.0*b*	60.3 ± 6.7*b*	49.4 ± 4.1*b*	0.819
nOPH10@GO	115.8 ± 2.7*a*	109.1 ± 8.3*a*	98.6 ± 3.5*a*	0.904

[a]All data are averages of three determinations with standard deviation. Means ± standard deviation. Means in a column with different letters are significantly different ($p < 0.05$) by the least significant difference test. [bT]he specific activity of native OPH was set to 100%. The loadings of OPH and nOPH10 on GO were both 0.64 mg mg^{-1}.

between the loading of OPH and surface hydrophobicity, and the adsorption of OPH on rGOs was governed by the hydrophobic interaction. To confirm this assumption, the effect of ionic strength on enzyme loading was studied. As presented in Figure 4E, when the NaCl concentration increased from 0.1 to 0.8 M, the loading of OPH improved correspondingly from 0.75 to 1.01 mg mg^{-1}, whereas that of nOPH10 did not change much. This trend illustrated that a high ionic strength environment benefited the interaction between OPH and rGOs. Such a phenomenon is similar to the principle of the hydrophobic separation resin, which is widely applied for protein separation. Proteins could adsorb on the hydrophobic separation resin in a high salt concentration buffer and are released from the resin by washing with a low salt concentration buffer.[10,41] The results suggested that the hydrophobic interaction was the driving force for the immobilization of OPH on rGOs.

However, OPH belongs to soluble proteins, there could not be a large hydrophobic area on its surface, and most of the hydrophobic residues are located in the interior of the enzyme near the active site.[35,42] Therefore, the loading of OPH on the hydrophobic rGOs might indicate that the change of structural conformation occurred during the adsorption between enzymes and supports. Figure 4F presents the circular dichroism (CD) spectra of the native OPH, OPH@GO, and nOPH10@GO, and the inset table shows the changes in secondary structures of enzyme before and after immobilization. Compared to native OPH, the contents of α-helix and β-sheet in OPH@GO decreased to 10.4 and 31.9%, respectively, and the content of the random coil increased to 43.2%. The secondary structures of nOPH10@GO showed no significant changes. The relatively high stable structure of the enzyme in nOPH10@GO could be attributed to the polymer shell covalently linked to the enzyme surface, which could stabilize the enzyme's conformation and protect its structure from deformation during the immobilization process. However, native OPHs did not have the protection from the polymer shell, for which their secondary structures were more likely to be changed. Therefore, the secondary structures of OPH@GO changed remarkably. The above results suggested that the interactions between enzymes and supports had a significant influence on the enzyme structure.

Figure 4D shows that nOPH10 loading gradually decreased with the increase in ζ-potential of rGOs. This result indicated that a higher negative potential was favorable for the immobilization of nOPH10, and the interaction between nOPH10 and GO could be regulated by the electrostatic attraction. Additionally, to further confirm the above interaction, we also synthesized a series of OPH nanocapsules ($nOPH10_{(1:3)}$, $nOPH10_{(2:2)}$, $nOPH10_{(3:1)}$, and $nOPH10_{(4:0)}$) with different surface charges by using different ratios of AAM and APM as comonomers. The loadings of these nanocapsules on GO gradually decreased with the increase in mass ratio of AAM/APM (Supporting Information, Figure S1), which could be attributed to the decrease in ζ-potential of OPH nanocapsules. Interestingly, $nOPH10_{(4:0)}$, which was synthesized using AAM as the only monomer and exhibited negative charge, was also immobilized on GO. Since the polymer shell is a polyacrylamide full of amino groups and the surface of GO is covered with oxygen-containing functional groups, it is highly possible that the interactions between the polymer shell and the GO surface could be due to hydrogen bonding.

3.4. Enzymatic Properties and Kinetic Parameters. As shown in Table 1, the specific activity of native OPH was 100%, and the relative activity of OPH@GO was reduced to 90.2%. The loss of relative activity for OPH@GO could be attributed to the fact that the conformation of OPH@GO changed remarkably compared to that of native OPH. As presented in Figure 4F, the contents of α-helix and β-sheet in OPH@GO decreased and that of the random coil increased. The change of enzyme structure had a negative influence on its activity. Table 1 shows that there was no significant difference in the Michaelis constant (K_m) between native OPH and nOPH10, which suggested that the polymer shell had little effect on K_m. The reason is that the introduced shell around the enzyme surface has extraordinary substrate permeability. Compared to native OPH (56.2 μM), the K_m values of OPH@GO and nOPH10@GO were significantly increased to 98.4 and 109.1 μM, respectively, indicating that the affinity between enzymes and substrates was decreased after the immobilization of native OPH and nOPH10 on GO. The above findings further indicated that the increase in K_m was mainly due to the immobilization of enzymes on GO.

Besides, the relative activity of nOPH10@GO (115.8%) was enhanced compared to native OPH. The catalytic constant (k_{cat}) of nOPH10@GO was increased (98.6 s^{-1}) compared to native OPH (47.5 s^{-1}), indicating the enhanced catalytic activity. Furthermore, the k_{cat}/K_m value of nOPH10@GO was higher than that of native OPH (0.904 vs 0.845 s^{-1} μM^{-1}), which suggested that nOPH10@GO possessed a relatively higher catalytic efficiency. The enhanced catalytic efficiency could be attributed to the synergistic effects between the amino group in the polymer shell and the hydroxyl group in GO supports. These two functional groups played a crucial role in governing the microenvironment around the enzyme, where the local pH may be higher due to the existence of monomer APM with a high $pK_a \approx 10$. Similar results regarding the increased local pH within the polymer shell were previously reported by Wei et al.[27]

3.5. Environmental Stability. The environmental stability of enzymes has a direct impact on its catalytic performance. Generally, the temperature, pH, and organic solvent in the environment can influence the catalytic activity of enzymes. Figure 5A exhibits the thermal stabilities of native OPH,

DOI: 10.1021/acsami.8b20744
ACS Appl. Mater. Interfaces 2019, 11, 11349−11359

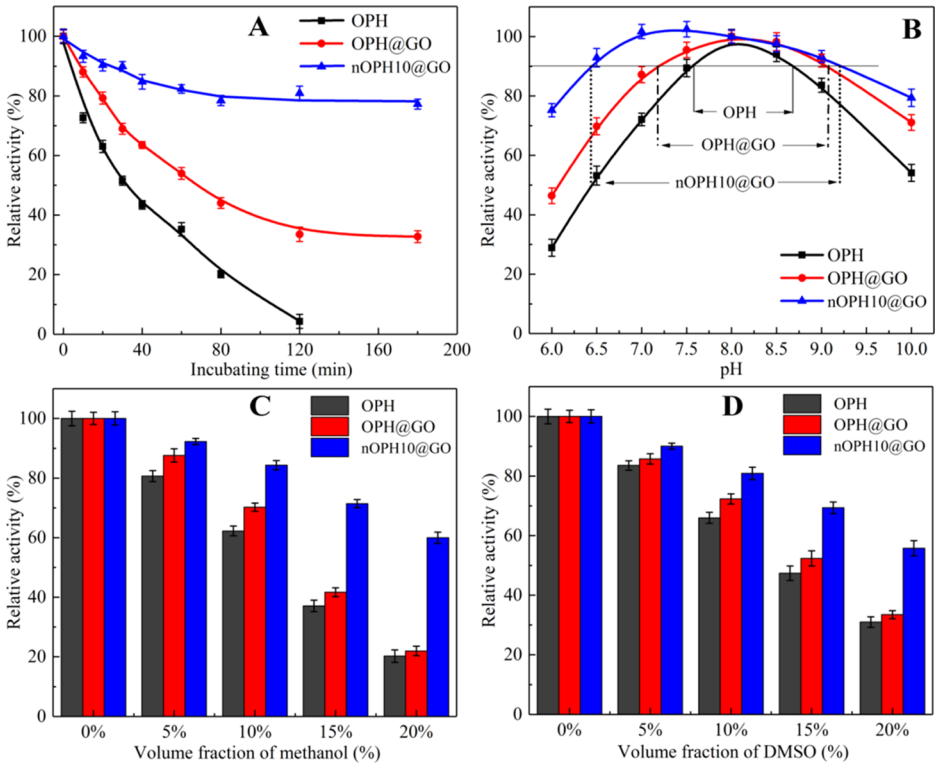

Figure 5. Relative activities of native OPH, OPH@GO, and nOPH10@GO incubated at 65 °C (A). Relative activities of native OPH, OPH@GO, and nOPH10@GO under various pHs (B) and subjected to different volume fractions of methanol (C) or DMSO (D) in 50 mM pH 8.0 PBS buffer solution. The loadings of OPH and nOPH10 on GO were both 0.64 mg mg^{-1}.

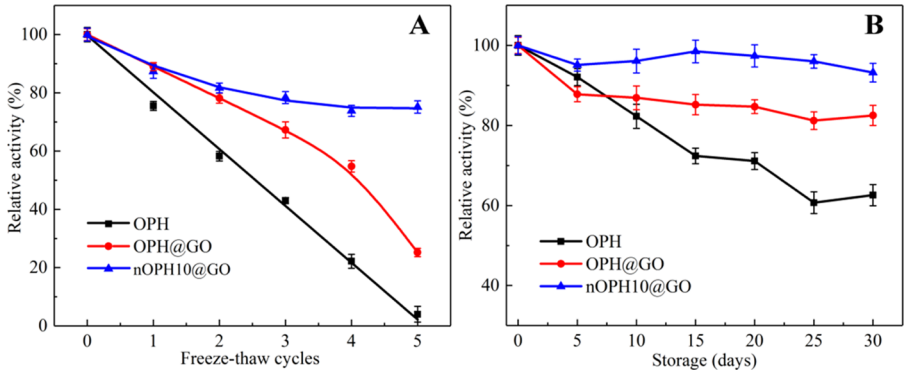

Figure 6. Freeze−thaw stabilities (A) and long-term storage stabilities (at 4 °C) (B) of native OPH, OPH@GO, and nOPH10@GO. The loadings of OPH and nOPH10 on GO were both 0.64 mg mg^{-1}.

OPH@GO, and nOPH10@GO at 65 °C. The nOPH10@GO exhibited a good thermal stability and kept about 80% of the original activity after incubating at 65 °C for 3 h. However, the native OPH almost lost the total activity after incubation for 2 h. The activity of OPH@GO decreased in the first 2 h and maintained about 40% of its original activity thereafter. The excellent thermal stability of nOPH10@GO could be attributed to the function of the polymer shell covalently linked to the enzyme surface, which can stabilize the OPH conformation and protect the enzyme structure from thermal effects. To confirm the stabilizing effect of the polymer shell, nOPHs with more covalent linkages between the core and the polymer shell were synthesized by grafting different amounts of NAS onto OPH. Figure S4 (Supporting Information, Figure S4) shows the relative activities of nOPH10@GO, nOPH30@GO, and nOPH50@GO after incubating at 65 °C for different times. As expected, the increase in the NAS/OPH molar ratio resulted in the gradual increase of the relative thermal stability, indicating that more covalent linkages between the OPH core and the polymer shell benefited the stabilization of OPH.

Besides the improved thermal stability, the nOPH10@GO exhibited a wider adaptability to pH compared to native OPH and OPH@GO. As shown in Figure 5B, the enzyme activities at pH 8.0 were set to 100%. The different vertical lines in Figure 5B indicate the pH ranges that the enzymes could maintain above 90% relative activity. Such pH ranges of native OPH, OPH@GO, and nOPH10@GO were about 7.6−8.7, 7.2−9.0, and 6.5−9.2, respectively, confirming that nOPH10@GO has a wider adaptability to pH. This outstanding performance could be ascribed to the synergistic effects between the amino group in the polymer shell and the hydroxyl group in the GO supports. These two functional

DOI: 10.1021/acsami.8b20744
ACS Appl. Mater. Interfaces 2019, 11, 11349−11359

groups may act as a buffer against the change of environmental pH and create a stable microenvironment for the enzyme.

Maintaining enzyme activity in a nonaqueous environment is challenging but holds great promise for a broad range of industrial and environmental applications. Here, methanol and DMSO were chosen to test the organic solvent stability of enzymes since these two organic solvents were widely used in the industry. These two organic solvents belong to polar organic solvents and would compete with water to form hydrogen bonding with protein backbones, thereby destroying protein conformation. As shown in Figure 5C,D, native OPH, OPH@GO, and nOPH10@GO presented different tolerances against the organic solvents, and the tolerance capacity followed the order nOPH10@GO > OPH@GO > OPH. When the volume fraction of methanol increased to 20%, the nOPH10@GO maintained about 60% of its original activity, nearly 3 times more than that of native OPH (20.3%) and OPH@GO (22.0%). Similar results were also found in the test with DMSO, indicating that nOPH10@GO had an improved stability in nonaqueous media. This was mainly because the hydrophilic polymer shell around the enzyme surface maintained a hydrophilic environment for OPH. This dual-immobilized enzyme system could meet the requirements for harsh industrial conditions and may enable application of more enzymes in the nonaqueous environment.

3.6. Storage Stability. The storage stability of enzymes has a great influence on their practical applications since an enzyme with relatively stable storage stability can dramatically lower the cost to store and replace the enzyme stocks and would bring more economic benefits.[27] As shown in Figure 6A, compared to native OPH, OPH@GO and nOPH10@GO exhibited more stable storage stability during the repeating freeze−thaw cycles. At the first two freeze−thaw cycles, the relative activities of OPH@GO and nOPH10@GO were both decreased and had no significant difference. However, this trend started to change from the third freeze−thaw cycle, after which the nOPH10@GO was more stable than OPH@GO. Specifically, the nOPH10@GO still maintained a higher activity of about 75% of its original activity after five freeze−thaw cycles, whereas the relative activity of OPH@GO decreased remarkably to only 20%. The results suggested that the immobilizing OPH on GO could improve the freeze−thaw stability to some extent, but such enhancement was far less than that of nOPH10@GO. The reason could be ascribed to the function of the polymer shell, which was covalently linked onto the OPH surface and could stabilize the OPH conformation against the detrimental effect of repeating freeze−thaw cycles.

Additionally, the long-term storage of enzymes was performed at 4 °C for 30 days. As shown in Figure 6B, the OPH activity gradually decreased and maintained about 60% of its original activity after 30 days. The OPH@GO was subjected to a loss of about 15% relative activity in the first 10 days of storage and maintained about 85% of its original activity thereafter. In comparison, the nOPH10@GO retained almost all activity throughout the 30 days. The prolonged shelf life of nOPH10@GO provides enormous advantages in industrial application, which can lower the costs in storage, handling, insurance, and administration.

3.7. Reusability. The reusability is one of the important parameters to assess the performance of immobilized enzymes in practical applications. Figure 7 shows the reusabilities of OPH@GO and nOPH10@GO. The relative activity of

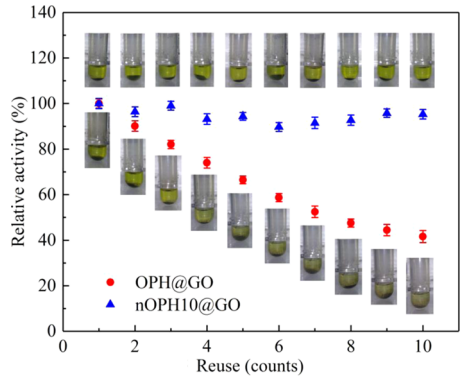

Figure 7. Reuse of OPH@GO and nOPH10@GO. The first round activity was set to 100%.

OPH@GO gradually decreased and maintained approximately 40% of its original activity after 10 times reuse. In contrast, the nOPH10@GO exhibited a fairly stable catalytic performance, and it still kept more than 90% of its original activity after 10 times reuse. This excellent reusability of nOPH10@GO could be due to the polymer shell around the enzyme surface, which could stabilize the enzyme's conformation and improve the operational stability. Compared to OPH@GO, in which the OPHs were naked on GO, the polymer shell protected the nOPH10@GO from various denaturation factors and provided numerous amino groups to interact with GO, which resulted in the improvement in stability and reusability of nOPH10@GO.

3.8. Biosensing. Here, the immobilized enzymes, OPH@GO and nOPH10@GO, were successfully applied to construct the biosensors (OPH@GO/GCE and nOPH10@GO/GCE), which were further employed to detect organophosphate pesticides. The detection mechanism was that the OPH catalyzed the hydrolysis of OPs to release *p*-nitrophenol (*p*-NP), which can be oxidized on the surface of the electrode.[33,43] As shown in Figure 8A, no prominent oxidation peaks were observed when using the bare GCE and GO/GCE to test the methyl parathion, suggesting that the OPs could not be hydrolyzed on their surface due to the lack of OPH. By comparison, when using the OPH@GO/GCE and nOPH10@GO/GCE, noticeable peaks at about 0.92 V were observed, and this was the oxidation evidence of the hydrolysis product (*p*-NP). It was worth noting that the oxidation peak of *p*-NP at nOPH10@GO/GCE was stronger than that of *p*-NP at OPH@GO/GCE, which could be attributed to the enhanced enzymatic activity of nOPH10@GO.

To further study the performance of the electrodes, OPH@GO/GCE and nOPH10@GO/GCE were exposed to different concentrations of methyl parathion. Figure 8B,C displays the concentration-dependent oxidation peak in the presence of 5−40 μM methyl parathions. It was clear that the oxidation peak intensity increased with the increase in the concentration of methyl parathion. Furthermore, the oxidation peaks obtained at nOPH10@GO/GCE were higher than that obtained at OPH@GO/GCE. Such sharper peaks would favor the detection of OPs.[34] Figure 8D presents the corresponding correlation between current readings and concentrations of methyl parathion. We could find that there was a good linear relationship between the concentration of methyl parathion and the responding current. More importantly, the peak currents of nOPH10@GO/GCE at different concentrations of methyl parathion were all greater than that of OPH@GO/

DOI: 10.1021/acsami.8b20744
ACS Appl. Mater. Interfaces 2019, 11, 11349−11359

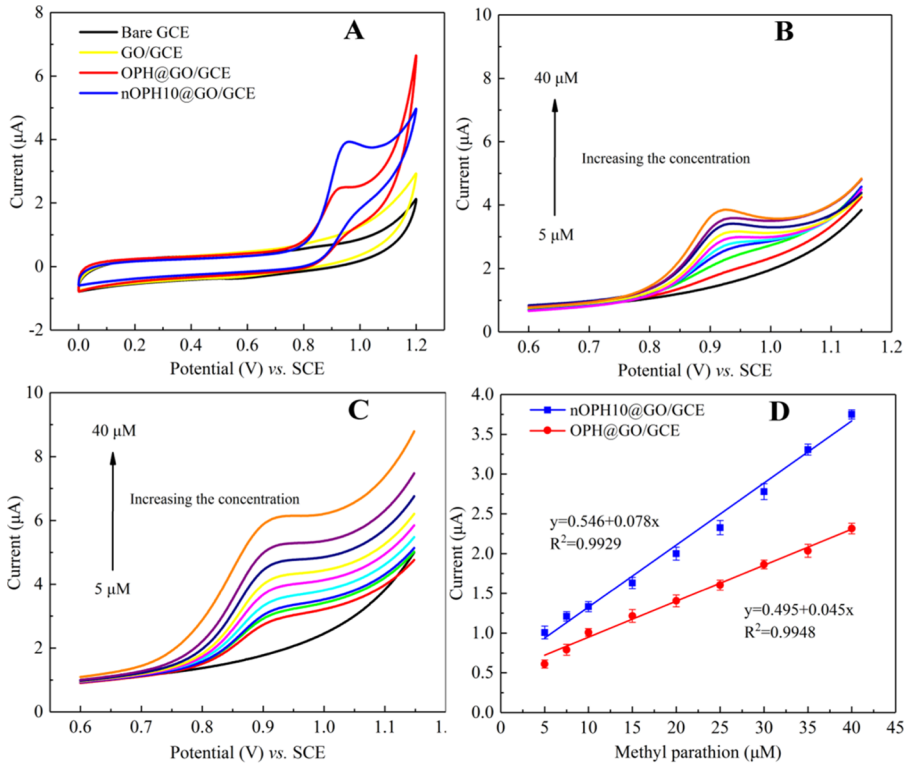

Figure 8. Cyclic voltammograms (CVs) of bare GCE, GO/GCE, OPH@GO/GCE, and nOPH10@GO/GCE in 0.05 M PBS (pH 7.4) containing 0.1 mM methyl parathion (A). CVs of OPH@GO/GCE (B) and nOPH10@GO/GCE (C) in 0.05 M PBS (pH 7.4) with different concentrations of methyl parathion (5−40 μM), and the corresponding correlations between current readings and concentrations of methyl parathion (D). The loadings of OPH and nOPH10 on GO were both 0.64 mg mg^{-1}.

GCE at the same condition, indicating that the nOPH10@GO/GCE had better detection performance compared with OPH@GO/GCE. These results demonstrated that the novel bioinorganic catalytic interface we constructed could improve the performance of the biosensor.

4. CONCLUSIONS

In conclusion, the proposed enzyme immobilization system, which combined the in situ radical polymerization technique with the noncovalent adsorption method to form the novel bioinorganic catalytic interface, exhibited enhanced enzymatic activity, environmental and storage stabilities as well as outstanding reusability compared with the native enzyme and the traditional immobilized enzyme. It was found that the nOPH10 was immobilized on GO mainly because of the electrostatic attraction, whereas the hydrophobic interaction was the driving force for the immobilization of OPH on rGOs. The introduced polymer shell around the enzyme surface provided abundant functional groups to interact with supports, thereby strengthening the interactions between them. The nOPH10@GO was further used to construct the biosensor, which presented better detection performance compared with OPH@GO/GCE. These findings provide the requisite data for the rational design of an appropriate enzyme immobilization platform that could enable enzymes to be used in harsh industrial processes and more fields.

■ ASSOCIATED CONTENT

Supporting Information

The Supporting Information is available free of charge on the ACS Publications website at DOI: 10.1021/acsami.8b20744.

ζ-Potentials, loadings of enzymes, representative TEM and AFM images, and thermal stability (PDF)

■ AUTHOR INFORMATION

Corresponding Author

*E-mail: zhgluo@scut.edu.cn. Tel.: +86-20-87113845. Fax: +86-20-87113848.

ORCID

Zhigang Luo: 0000-0001-7549-8083

Notes

The authors declare no competing financial interest.

■ ACKNOWLEDGMENTS

This research was supported by National Natural Science Foundation of China (21878106, 21576098), Fundamental Research Funds for the Central Universities, SCUT (2018KZ08), National Key R&D Program of China (2018YFD0401003), 111 Project (B17018), Key Project of Science and Technology of Guangdong Province (2018A050506016, 2017B090901002), and China Postdoctoral Science Foundation (2017T100616, 2016M590787).

■ REFERENCES

(1) Zhang, Y.; Ge, J.; Liu, Z. Enhanced Activity of Immobilized or Chemically Modified Enzymes. *ACS Catal.* **2015**, *5*, 4503−4513.

(2) Rodrigues, R. C.; Ortiz, C.; BerenguerMurcia, Á.; Torres, R.; Fernándezlafuente, R. Modifying enzyme activity and selectivity by immobilization. *Chem. Soc. Rev.* **2013**, *42*, 6290−6307.

(3) Feng, D.; Liu, T. F.; Su, J.; Bosch, M.; Wei, Z.; Wan, W.; Yuan, D.; Chen, Y. P.; Wang, X.; Wang, K. Stable metal-organic frameworks

containing single-molecule traps for enzyme encapsulation. *Nat. Commun.* **2015**, *6*, No. 5979.
(4) Cantone, S.; Ferrario, V.; Corici, L.; Ebert, C.; Fattor, D.; Spizzo, P.; Gardossi, L. Efficient immobilisation of industrial biocatalysts: criteria and constraints for the selection of organic polymeric carriers and immobilisation methods. *Chem. Soc. Rev.* **2013**, *42*, 6262−6276.
(5) Cao, L. Immobilised enzymes: science or art? *Curr. Opin. Chem. Biol.* **2005**, *9*, 217−226.
(6) Sigurdardóttir, S. B.; Lehmann, J.; Ovtar, S.; Grivel, J. C.; Negra, M. D.; Kaiser, A.; Pinelo, M. Enzyme Immobilization on Inorganic Surfaces for Membrane Reactor Applications: Mass Transfer Challenges, Enzyme Leakage and Reuse of Materials. *Adv. Synth. Catal.* **2018**, *360*, 2578−2607.
(7) José, C.; Toledo, M. V.; Nicolas, P.; Lassalle, V. L.; Ferreira, M. L.; Briand, L. E. Influence of the nature of the support in the catalytic performance of CALB: experimental and theoretical evidences. *Catal. Sci. Technol.* **2018**, *8*, 3513−3526.
(8) Hartmann, M.; Kostrov, X. Immobilization of enzymes on porous silicas-benefits and challenges. *Chem. Soc. Rev.* **2013**, *42*, 6277−6289.
(9) Zhao, F.; Li, H.; Jiang, Y.; Wang, X.; Mu, X. Co-immobilization of multi-enzyme on control-reduced graphene oxide by non-covalent bonds: an artificial biocatalytic system for the one-pot production of gluconic acid from starch. *Green Chem.* **2014**, *16*, 2558−2565.
(10) Zhang, Y.; Zhang, J.; Huang, X.; Zhou, X.; Wu, H.; Guo, S. Assembly of graphene oxide-enzyme conjugates through hydrophobic interaction. *Small* **2012**, *8*, 154−159.
(11) Zhang, J.; Feng, Z.; Haijun, Y.; Xuelei, H.; Hui, L.; Jingyan, Z.; Shouwu, G. Graphene oxide as a matrix for enzyme immobilization. *Langmuir* **2010**, *26*, 6083−5.
(12) Liu, Z.; Robinson, J. T.; Sun, X.; Dai, H. PEGylated Nanographene Oxide for Delivery of Water-Insoluble Cancer Drugs. *J. Am. Chem. Soc.* **2008**, *130*, 10876−10877.
(13) Zeng, Q.; Cheng, J.; Tang, L.; Liu, X.; Liu, Y.; Li, J.; Jiang, J. Self-Assembled Graphene−Enzyme Hierarchical Nanostructures for Electrochemical Biosensing. *Adv. Funct. Mater.* **2010**, *20*, 3366−3372.
(14) Bepete, G.; Anglaret, E.; Ortolani, L.; Morandi, V.; Huang, K.; Pénicaud, A.; Drummond, C. Surfactant-free single-layer graphene in water. *Nat. Chem.* **2016**, *9*, 347.
(15) Qi, L.; Luo, Z.; Lu, X. Facile Synthesis of Starch-Based Nanoparticles Stabilized Pickering Emulsion: Its pH-Responsive Behavior and Application for the Recyclable Catalysis. *Green Chem.* **2018**, *20*, 1538−1550.
(16) Polshettiwar, V.; Varma, R. S. Green chemistry by nano-catalysis. *Green Chem.* **2010**, *12*, 743−754.
(17) Bell, A. T. The Impact of Nanoscience on Heterogeneous Catalysis. *Science* **2003**, *299*, 1688−1691.
(18) Küchler, A.; Yoshimoto, M.; Mavelli, F.; et al. Enzymatic reactions in confined environments. *Nat. Nanotechnol.* **2016**, *11*, 409−420.
(19) Huang, W. C.; Wei, W.; Xue, C.; Mao, X. Effective Enzyme Immobilization onto a Magnetic Chitin Nanofiber Composite. *ACS Sustainable Chem. Eng.* **2018**, *6*, 8118−8124.
(20) Sheldon, R. A. Enzyme immobilization: the quest for optimum performance. *Adv. Synth. Catal.* **2007**, *349*, 1289−1307.
(21) Stepankova, V.; Bidmanova, S.; Koudelakova, T.; Prokop, Z.; Chaloupkova, R.; Damborsky, J. Strategies for Stabilization of Enzymes in Organic Solvents. *ACS Catal.* **2013**, *3*, 2823−2836.
(22) Tran, D. N.; Balkus, K. J. Perspective of Recent Progress in Immobilization of Enzymes. *ACS Catal.* **2011**, *1*, 956−968.
(23) Tully, J.; Yendluri, R.; Lvov, Y. Halloysite Clay Nanotubes for Enzyme Immobilization. *Biomacromolecules* **2016**, *17*, 615−621.
(24) Schmid, A.; Dordick, J. S.; Hauer, B.; Kiener, A.; Wubbolts, M.; Witholt, B. Industrial biocatalysis today and tomorrow. *Nature* **2001**, *409*, 258−268.
(25) Hanefeld, U.; Gardossi, L.; Magner, E. Understanding enzyme immobilisation. *Chem. Soc. Rev.* **2009**, *38*, 453−468.
(26) Lian, X.; Fang, Y.; Joseph, E.; Wang, Q.; Li, J.; Banerjee, S.; Lollar, C.; Wang, X.; Zhou, H. C. Enzyme-MOF (metal-organic framework) composites. *Chem. Soc. Rev.* **2017**, *46*, 3386−3401.
(27) Wei, W.; et al. Construction of robust enzyme nanocapsules for effective organophosphate decontamination, detoxification, and protection. *Adv. Mater.* **2013**, *25*, 2212−2218.
(28) Liu, Y.; Du, J.; Yan, M.; Lau, M. Y.; Hu, J.; Han, H.; Yang, O. O.; Liang, S.; Wei, W.; Wang, H.; et al. Biomimetic enzyme nanocomplexes and their use as antidotes and preventive measures for alcohol intoxication. *Nat. Nanotechnol.* **2013**, *8*, 187−192.
(29) Li, J.; Jin, X.; Liu, Y.; Li, F.; Zhang, L.; Zhu, X.; Lu, Y. Robust enzyme-silica composites made from enzyme nanocapsules. *Chem. Commun.* **2015**, *51*, 9628−9631.
(30) Omburo, G. A.; Kuo, J. M.; Mullins, L. S.; Raushel, F. M. Characterization of the zinc binding site of bacterial phosphotriesterase. *J. Biol. Chem.* **1992**, *267*, 13278−13283.
(31) Hummers, W. S.; Offeman, R. E. Preparation of Graphitic Oxide. *J. Am. Chem. Soc.* **1958**, *80*, 1339.
(32) Stankovich, S.; Dikin, D. A.; Dommett, G. H. B.; Kohlhaas, K. M.; Zimney, E. J.; Stach, E. A.; Piner, R. D.; Nguyen, S. T.; Ruoff, R. S. Graphene-based composite materials. *Nature* **2006**, *442*, 282−286.
(33) Tang, X.; Zhang, T.; Liang, B.; Han, D.; Zeng, L.; Zheng, C.; Li, T.; Wei, M.; Liu, A. Sensitive electrochemical microbial biosensor for p-nitrophenylorganophosphates based on electrode modified with cell surface-displayed organophosphorus hydrolase and ordered mesopore carbons. *Biosens. Bioelectron.* **2014**, *60*, 137−142.
(34) Bao, J.; Hou, C.; Dong, Q.; Ma, X.; Chen, J.; Huo, D.; Mei, Y.; Galil, K. H. A. E.; Chen, W.; Yu, L. ELP-OPH/BSA/TiO 2 nanofibers/c-MWCNTs based biosensor for sensitive and selective determination of p-nitrophenyl substituted organophosphate pesticides in aqueous system. *Biosens. Bioelectron.* **2016**, *85*, 935−942.
(35) Dong, Y. J.; Bartlam, M.; Sun, L.; Zhou, Y. F.; Zhang, Z. P.; Zhang, C. G.; Rao, Z.; Zhang, X. E. Crystal structure of methyl parathion hydrolase from Pseudomonas sp. WBC-3. *J. Mol. Biol.* **2005**, *353*, 655−663.
(36) Chang, S. K. C.; Yan, Z. *Protein Analysis, Food Analysis*; Springer: Cham, 2017; pp 315−331.
(37) Watson, M. L. Staining of Tissue Sections for Electron Microscopy with Heavy Metals. *J. Cell Biol.* **1958**, *4*, 475−478.
(38) Benning, M. M.; Kuo, J. M.; Raushel, F. M.; Holden, H. M. Three-Dimensional Structure of Phosphotriesterase: An Enzyme Capable of Detoxifying Organophosphate Nerve Agents. *Biochemistry* **1994**, *33*, 15001−15007.
(39) Wen, J.; Anderson, S. M.; Du, J.; Yan, M.; Wang, J.; Shen, M.; Lu, Y.; Segura, T. Controlled Protein Delivery Based on Enzyme-Responsive Nanocapsules. *Adv. Mater.* **2011**, *23*, 4549−4553.
(40) Si, Y.; Samulski, E. T. Synthesis of water soluble graphene. *Nano Lett.* **2008**, *8*, 1679−1682.
(41) Jennissen, H. P. Hydrophobic interaction chromatography: harnessing multivalent protein-surface interactions for purification procedures. *Methods Mol. Biol.* **2005**, *305*, 81−99.
(42) Grimsley, J. K.; Martin Scholtz, J.; Nick Pace, C.; Wild, J. R. Organophosphorus Hydrolase Is a Remarkably Stable Enzyme That Unfolds through a Homodimeric Intermediate†. *Biochemistry* **1997**, *36*, 14366−14374.
(43) Zhang, T.; Lang, Q.; Zeng, L.; Li, T.; Wei, M.; Liu, A. Substituent effect on the oxidation peak potentials of phenol derivatives at ordered mesoporous carbons modified electrode and its application in determination of acidity coefficients (pKa). *Electrochim. Acta* **2014**, *115*, 283−289.

DOI: 10.1021/acsami.8b20744
ACS Appl. Mater. Interfaces 2019, 11, 11349−11359